

Vortex-induced vibration characteristics of a low-mass-ratio flexible cylinder

Lee Kee Quen^{*1}, Aminudin Abu¹, Naomi Kato², Pauziah Muhamad¹, Kang Hooi Siang^{3,6},
Lim Meng Hee⁴ and Mohd Asamudin A Rahman⁵

¹Malaysia-Japan International Institute of Technology, Universiti Teknologi Malaysia, Kuala Lumpur, 54100 Malaysia

²Department of Naval Architecture and Ocean Engineering, Graduate School of Engineering, Osaka University, Japan

³School of Mechanical Engineering, Universiti Teknologi Malaysia, Malaysia

⁴Institute of Noise and Vibration, Universiti Teknologi Malaysia, Kuala Lumpur, Malaysia

⁵School of Ocean Engineering, Universiti Malaysia Terengganu, Terengganu 21030, Malaysia

⁶Marine Technology Center, Institute for Vehicle System and Engineering, Universiti Teknologi Malaysia, Malaysia

(Received July 24, 2019, Revised March 30, 2020, Accepted April 3, 2020)

Abstract. A laboratory experiment is conducted to investigate the behaviour of a low-mass-ratio and high aspect ratio flexible cylinder under vortex-induced vibration (VIV). A flexible cylinder with aspect ratio of 100 and mass ratio of 1.17 is towed horizontally to generate uniform flow profile. The range of Reynolds number is from 1380 to 13800. Vibration amplitude, in-line and cross-flow frequency response, amplitude trajectory, mean tension variation and hydrodynamic force coefficients are analyzed based on the measurement from strain gauges, load cell and CCD camera. Experimental results indicate that broad-banded lock-in region is found for the cylinder with a small Strouhal number. The frequency switches in the present study indicates the change of the VIV phenomenon. The hydrodynamic force responses provide more understanding on the VIV of a low mass ratio cylinder.

Keywords: vortex-induced vibration; low mass ratio; high aspect ratio; flexible cylinder

1. Introduction

The phenomenon of vortex-induced vibration (VIV) has been studied for long. It was as early as 60's that the research had been performed by the offshore industry in order to improve the design of risers and offshore structures. To name few, Roshko (1961), Feng (1968), Kato (1982), Williamson and Roshko (1988), Vikestad *et al.* (2000), Vandiver *et al.* (2009), Quen *et al.* (2014), Kim *et al.* (2015), Rahman *et al.* (2016), Jeong *et al.* (2016), Kang *et al.* (2017), Ji *et al.* (2018) and Chen *et al.* (2019) are among the works that can be found in the literatures. Based on the previous studies, it can be noticed that most of them are focused on cylinder with one degree of freedom, where the cylinder is allowed to vibrate in transverse direction only. Cylinder with two degree of freedom is started to be studied recently because of the demand from the offshore industries. Because of the significance of the dynamic behaviors, the VIV of a rigid circular cylinder has been studied extensively, and it is still on going. Aguirre (1978) can be considered as the pioneer in characterizing the streamwise VIV. A wake-oscillator model was then introduced by Currie and Turnbull (1987) in predicting the VIV response of a cylinder. Another comprehensive study on the change of the natural frequency ratio from 1 to 2 had been conducted on an elastically mounted rigid cylinder by Dahl *et al.* (2006). They found that by increasing the natural frequency ratio, the CF amplitude profile reduced

significantly from 1.5 to around 1. Bearman (2011), Dahl *et al.* (2010) and Assi (2009), on the other hand, pointed out that the ratio of the IL to CF frequency of a cylinder which was vibrating was precisely at 2. Besides, high repeatable, stable and persisting 8-shape trajectory was well-defined at the lock-in region, as reported in Sanchis *et al.* (2008) and Gonçalves *et al.* (2013). The accuracy and feasibility of the large eddy simulation in three dimensional unsteady flow is examined by Jus *et al.* (2014) to identify the VIV response on an elastically mounted cylinder. Jauvtis and Williamson (2003) and Williamson and Govardhan (2008) indicated that the amplitude response of the cylinder in 2dof with mass ratio, $m^* > 6$ remains the same as the cylinder which is allowed to vibrate in CF direction only. However, as the $m^* < 6$, dramatic change was observed, where a "super-upper" branch was produced with very high amplitude response.

In the application of offshore engineering, floating structures such as drilling ships and oil rigs may use a long cylindrical structure as drilling riser to connect the structures to the ocean floor. As the exploration of the oil resources have moved into deeper seabed, a longer riser is required. This slender and long riser, which can be regarded as high aspect ratio cylinder, is highly susceptible to VIV (Dahl, 2008). A cylinder can be characterized as high aspect ratio cylinder if the submerged length (L) is much higher than the diameter of the cylinder (D), where $L/D > 13$, according to Jauvtis and Williamson (2004).

It is a challenging and creative task to design a marine riser that enduring extreme offshore environmental conditions (Branković and Bearman, 2006). However, currently only a few researchers have focused on the

*Corresponding author, Ph.D.
E-mail: lkquen@utm.my

dynamic mechanism of VIV on a slender and flexible cylinder. Vandiver and Tae (1988) conducted one of the earliest investigations that focused on the characteristic of flexible riser. The experiment revealed that the number of modes due to the shear flow excitation was found to be a useful non-dimensional parameter compared to the shear steepness. Shear steepness denotes the current of the shear flow whether it is a strong or weak. Boom and Walree (1990), on the other hand, further investigated the hydrodynamic features of flexible riser with aspect ratio of 50 numerically. In the study, the ratio of the drag force frequency to the transverse force frequency was found to be two for a flexible riser. Vandiver (1993) proposed several useful parameters in predicting the vortex-induced vibration, especially during the lock-in condition of a long and flexible cylinder. Huera-Huarte and Bearman (2009) utilized various top-tensions on cylinder with aspect ratio of 94 to ascertain its dynamic responses. The findings in the study were interesting where the flexible cylinder behaved similar to a rigid cylinder under low tension, while it performed like a cable when the tension increased. Xu *et al.* (2009) investigated the behaviour of dominant vortex modes in riser's response under range of subcritical Reynolds number. Wu *et al.* (2016) investigated the interaction between the inline and cross-flow response of a flexible cylinder, and noticed that traveling waves are able to influence the motion phase angle of the cylinder. The latest research by Xu *et al.* (2018) discovered two detached branches at first and second excitation regions, respectively, which is similar with an elastically-mounted rigid cylinder. Up to now, the dynamic response of VIV of a flexible cylinder, specifically with low mass ratio and large aspect ratio, is still lacking. Therefore, the present study aims to investigate the dynamic response of a low mass ratio and high aspect ratio flexible cylinder. The purpose is to understand comprehensively the behaviour of a flexible cylinder under VIV from several aspects, which include (1) the vibration amplitude (2) the IL and CF frequency response (3) amplitude trajectory (4) mean tension variation and (5) hydrodynamic force coefficients.

2. Methodology

2.1 Experimental Set-up

The experiment was conducted in the towing tank of the Department of Naval Architecture and Ocean Engineering of Osaka University. It has a 100 m long water channel, with width of 7.8 m and depth of 4.35 m. A poly vinyl chloride (PVC) cylinder is used as the riser model, with the settings as detailed in Table 1. The flexible cylinder is designed to move freely in an axial direction at one end and in restricted torsion effect with at both ends. At the moveable end, a pre-tension force of 147N is applied to produce a tension-dominated model. In general, a pre-tension that 1.3 times of the submerged weight of the riser will be used, $T = 1.3W_aL$, where T , W_a and L denote the pre-tension, the submerged weight of the riser per unit length and the length of riser, respectively (Kuiper, 2008). The

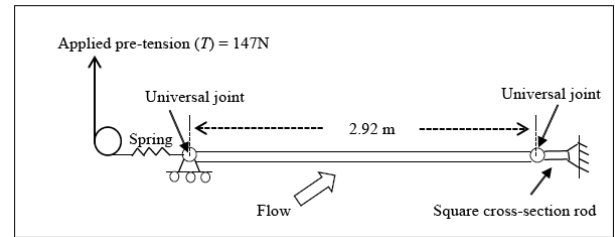


Fig. 1a schematic diagram of the experimental set up

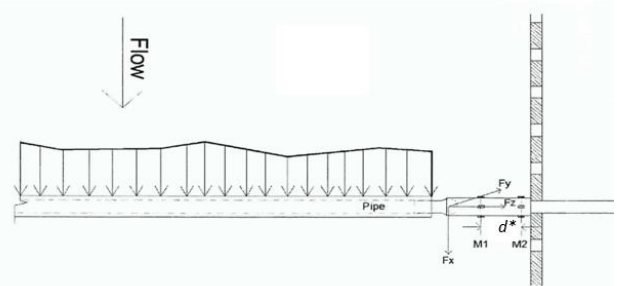


Fig. 1b Schematic diagram of the location of strain gauges and the bending strains of two adjacent measurement stations (M1 and M2)

minimum calculated pre-tension that can be used in the present study by referring to the equation is 11 N. However, in order to generate a more tension dominated model, the pre-tension was set to be 147 N before the start of each run. This pre-tension value is referred to the studies of Huera-Huarte and Bearman (2009a), Chaplin *et al.* (2005) and Sanaati and Kato (2012). To allow the cylinder to bend in inline (IL) and cross-flow (CF) directions, universal joints are used at the both ends of the cylinder. Fig. 1a shows the schematic diagram of the model set up. The cylinder is placed at a 0.35m depth from the water surface level, and is towed to create uniform flow speed. The speed is operated between 0.1-1.0 m/s, with a step increment of 0.03 m/s.

2.2 Measurement System

The vibration and frequency responses are recorded using two CCD cameras, which are installed about 18 diameter downstream and above of the cylinder to avoid wake interference. To sufficiently capture the motion of the cylinder, camera sampling rate of 30 Hz is utilized. Only the mid-span point was used as the target to be captured by the CCD camera. Hence, in the present study, large amplitude response can only be captured for the odd modes (first mode, third mode, fifth mode) by the CCD camera. To obtain the amplitude response from the CCD camera, the video data from the two CCD cameras needed to be converted into sequence of still images in form of bitmap image firstly. Then, these still images from the two cameras needed to be synchronized before transforming into the measured points. The transformation data of two cameras was done simultaneously by using commercial motion tracking software. Calibration of the camera has been done and the largest discrepancy of the measured data is less than 5%.

Table 1 Parameters of riser

Outer diameter (D)	18 mm
Inner diameter (d)	13 mm
Length (L)	2.92 m
Pre-tension (T)	147N
Bending Stiffness (EI)	9.0Nm ²
Spring Stiffness (k _s)	6.5N/m
Cylinder axial stiffness (EA/L)	100 N/mm
Cylinder air weight	1.64 N/m
Total weight including internal water (m)	2.97N/m
Mass ratio	1.17
Damping ratio (z)	0.028
Flow speed (U)	0.1-1.0 m/s
Subcritical Reynolds number range (Re)	1380-13,800
Natural frequency in still water, f _n	2.92 Hz

The hydrodynamic force coefficients, on the other hand, are obtained through four pairs of strain gauges, which are installed at the square cross-section rod located at the fix end of the cylinder, as shown in Fig. 1b. The sampling rate is 200 Hz with a low-pass filter of 100Hz cut-off frequency to filter unavoidable noise during the experiment. The hydrodynamic force values can be obtained by taking the difference between the bending moment strains of two adjacent measurement stations (M1 and M2 in Fig. 1b) and divided by the specified distance, d* (equation 1 and 2) and calibration coefficients. The calibration coefficients are obtained via calibration tests using a pulley-weight system. The purpose is to convert the bending moment strain of DC volts into Newton meter (Nm). The subscripts of x and y represent the IL and CF directions, respectively. Then, by using equations 5, 6 and 7 for IL and CF forces respectively, the mean drag, fluctuating drag and fluctuating lift force coefficients can be calculated.

$$F_d = (M1_x - M2_x) / d^* \quad (1)$$

$$F_l = (M1_y - M2_y) / d^* \quad (2)$$

Tension load cell with capacity of 1000 N is used to capture the mean tension variation of the cylinder. Similar to the strain gauges, the sampling rate of the tension load cell is 200 Hz with 100Hz low-pass cut-off frequency. The detail experiment information can be obtained in Sanaati's description (Sanaati 2012).

3. Results and discussions

3.1 Cross-flow amplitude response

In general, the dynamic responses of a cylinder can be represented by non-dimensional cross-flow (CF) amplitude ratio, A* against reduced velocity, V_r, where A* can be obtained by taking the time series displacement in standard deviation divided by the cylinder's diameter, A* = A_{std} / D while V_r is the non-dimensional velocity, V_r = U / f_n D. The amplitude ratio (A*) of the present study is obtained from the mid-span point of the cylinder. Fig. 2a shows the

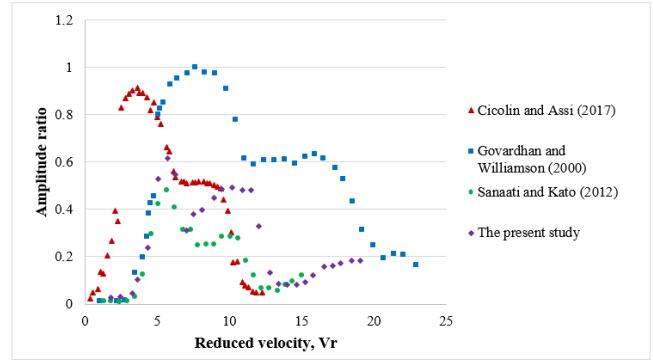


Fig. 2a Comparison of the amplitude response with previous studies

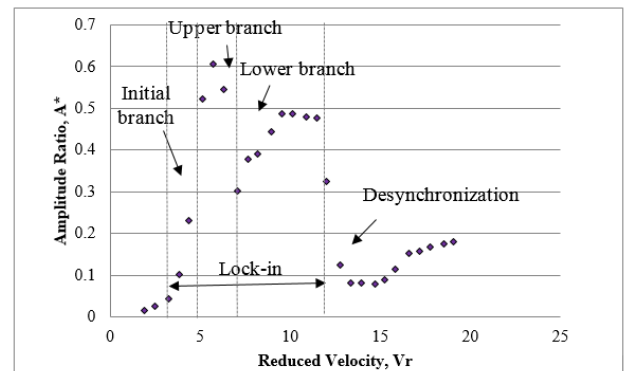


Fig. 2b The CF amplitude ratio of a low mass ratio flexible cylinder

validation of the present study in term of amplitude ratio with the other studies (Cicolin and Assi, 2017; Govardhan and Williamson, 2000; Sanaati and Kato, 2012) while fig. 2b shows the CF amplitude ratio of a low mass ratio flexible cylinder with branches classification at various reduced velocities. For a low mass ratio cylinder, four branches namely the initial, upper, lower and desynchronization branches are noticed in the amplitude trend. It is dissimilar to a high mass ratio cylinder that only displays two branches (initial and lower branches) based on the literature. The presence of these branches was also displayed in Korkischko and Meneghini (2010) and Branković and Bearman (2006). It is suggested that this phenomenon is highly influenced by the parameter of mass ratio (m*).

Besides, compared to a cylinder of high mass ratio (m* > 10) which has a narrow lock-in region (5 < V_r < 7.5) (Blevin and Coughran, 2009), the synchronization region of a low mass ratio cylinder is broad-banded (3.2 < V_r < 11.5), as shown in Fig. 2b. Similar circumstance was also reported by Khalak and Williamson (1997) and Branković and Bearman (2006). It is explained that a light-weight cylinder is influenced by the added mass effects. According to Khalak and Williamson (1999), the increase of reduced velocity reduces the added mass and hence results in more increment on the apparent natural frequency. Hence, a broader range of lock-in region is produced. More detail explanations about this statement can be found in the following section (section 3.2).

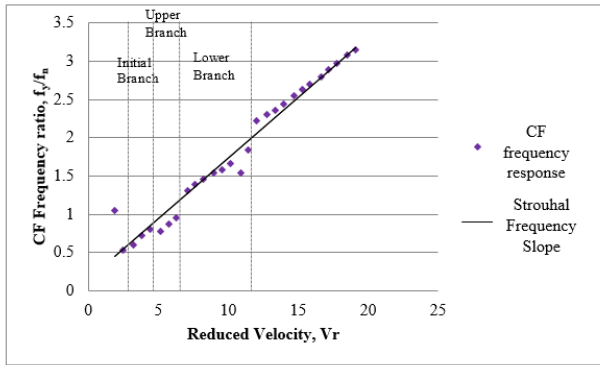


Fig. 3 The CF frequency response of a low mass ratio flexible cylinder

3.2 Frequency response

Fig. 3 indicates the cross-flow (CF) frequency response data of a low mass ratio flexible cylinder in the present experiment. The frequency ratios (CF in Fig. 3 and in-line (IL) in Fig. 4) are obtained by dividing those frequency responses with the still water natural frequency (f_n) of the cylinder. By using Fast Fourier Transform (FFT), only the dominant frequency is taken into account based on the hydrodynamic force data in time series. The Strouhal number, St , which is the non-dimensional vortex shedding frequency, can be obtained by assuming that the frequency of the cylinder is reacting the same as the vortex shedding frequency (Huera-Huarte, 2006). It is found to be 0.158 based on the linear fit of slope for the cylinder (Fig. 3). This value is slightly smaller than a rigid cylinder of 0.2 (Norberg, 2001; Lee *et al.* 2013). However, good agreement was found in Huera Huarte (2006) for a flexible cylinder.

Based on Fig. 3, it is interesting to observe that the CF shedding frequency ratio during the lock-in phenomenon from $V_r = 3.2$ to 11.5 is not remained at one (shedding frequency is not locked into the natural frequency) as for the cylinder with high mass ratio. This condition can be explained by following: In the present study, the CF shedding frequency is normalized with the still water natural frequency of flexible cylinder. According to Gabbai and Benaroya (2005), the oscillation frequency over a wide range of velocity is the apparent natural frequency ($f_{Tn}(V_r)$), and this frequency is in inverse relationship with the added mass based on the proposed equation:

$$f_{Tn}(V_r) = \frac{1}{2\pi} \sqrt{\frac{k}{m + c_{EA}(V_r)m_d}} \quad (3)$$

where m_d denotes the displaced mass of fluid, $m_d = \pi\rho D^2/4$, m is the cylinder mass without the added mass effect, k is the spring stiffness and c_{EA} is the effective added-mass coefficient. The authors reported that the increase of reduced velocity decreases the added mass and hence increases the apparent natural frequency. Therefore, in the present study, the CF shedding frequency is locked on the apparent natural frequency starting at $V_r = 3.2$. As the reduced velocity increases, the apparent natural

frequency increases. The lock-in persisted up to $V_r = 11.5$. Vikestad *et al.* (2000) reported that the narrower lock-in region of high mass ratio cylinder is due to the small variation of added mass resulting from the less increment of the apparent natural frequency. Cylinder with different mass ratio will have a similar lock-in region if the reduced velocity is defined based on the apparent natural frequency (Govardhan and Williamson, 2000). However, in the present study, only still water natural frequency is used to express the reduced velocity for the purpose of reporting the experimental data.

3.3 Relationship between amplitude and frequency responses

In this section, both the amplitude and frequency responses are combined to examine the relationship between them. To ascertain the relationship of the CF and IL response, the IL-to-CF frequency ratio is investigated as well.

Based on Fig. 4, it can be seen that good correlation is found between the amplitude ratio and the frequency responses of the cylinder. At the initial and upper branch of amplitude ($3.2 < V_r < 6.3$), the IL-to-CF ratio fluctuates from 4 to 3. Similar condition was also reported by Huse *et al.* (2002) where IL-to-CF ratio as high as 4 was observed in low reduced velocity region. According to Huse *et al.* (2002), the effect of IL frequency towards to CF response was insignificant if the IL frequency was not twice of CF frequency. However, present study shows that the constant IL-to-CF ratio of 3 from $V_r = 4.4$ to $V_r = 5.7$ contributes to the maximum amplitude ratio of bare cylinder at $V_r = 5.7$. In fact Marcollo and Hinwood (2006) stated that the large IL-to-CF frequency ratio indicates the support of IL dominant mode towards the dominance of CF response.

A secondary peak of amplitude ratio is found in the lower branch after the maximum vibration amplitude (Fig. 3). At this stage, the IL frequencies are twice of CF frequencies. The IL-to-CF ratio of 2 remains the same throughout the entire velocity region starting from $V_r = 6.3$, including the secondary lock-in ($12 < V_r < 19$) where the response is periodic, denoting the creation of regular vortices. The secondary lock-in mentioned here denotes the lock-in of the second CF mode. The reduction of amplitude ratio at $V_r = 12$ is due to the simultaneous switch of IL and CF frequencies into second and fourth mode respectively, where node instead of anti-node is captured at the center of the cylinder.

Based on Fig. 4, it can be seen that each of the switch of frequency denotes the change of the VIV phenomenon, where the first jump of frequency at $V_r = 3.2$ denotes the entering of CF lock-in region. The second jump of frequency at $V_r = 7$ leads to the switch of amplitude branch, while the formation of high mode vibration is the result of the third switch of frequency at $V_r = 12$. This indicates that the jump of frequency is usually takes place at the transition between different behaviours of VIV phenomenon. The similar condition is also reported by Sanaati (2012). In general, the jump of the frequency occurs in IL and CF directions and most of the time, both of them respond simultaneously.

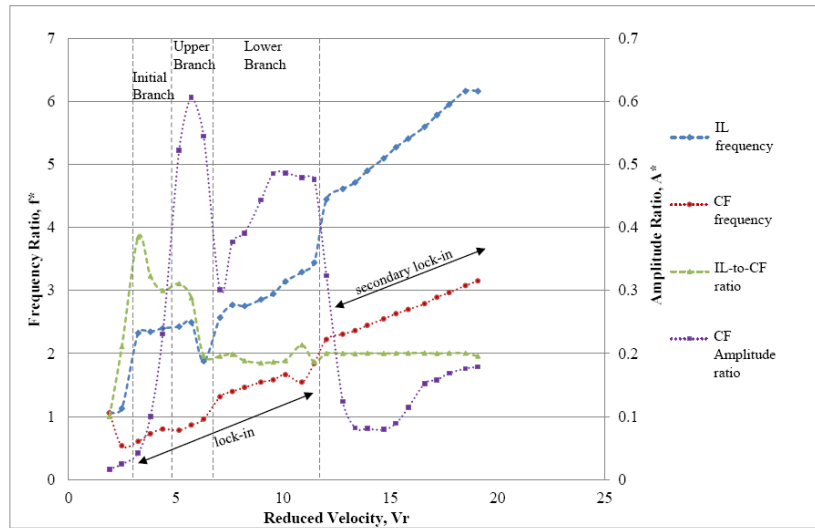


Fig. 4 IL, CF frequency ratio and IL-to-CF ratio along with CF vibration amplitude of bare cylinder

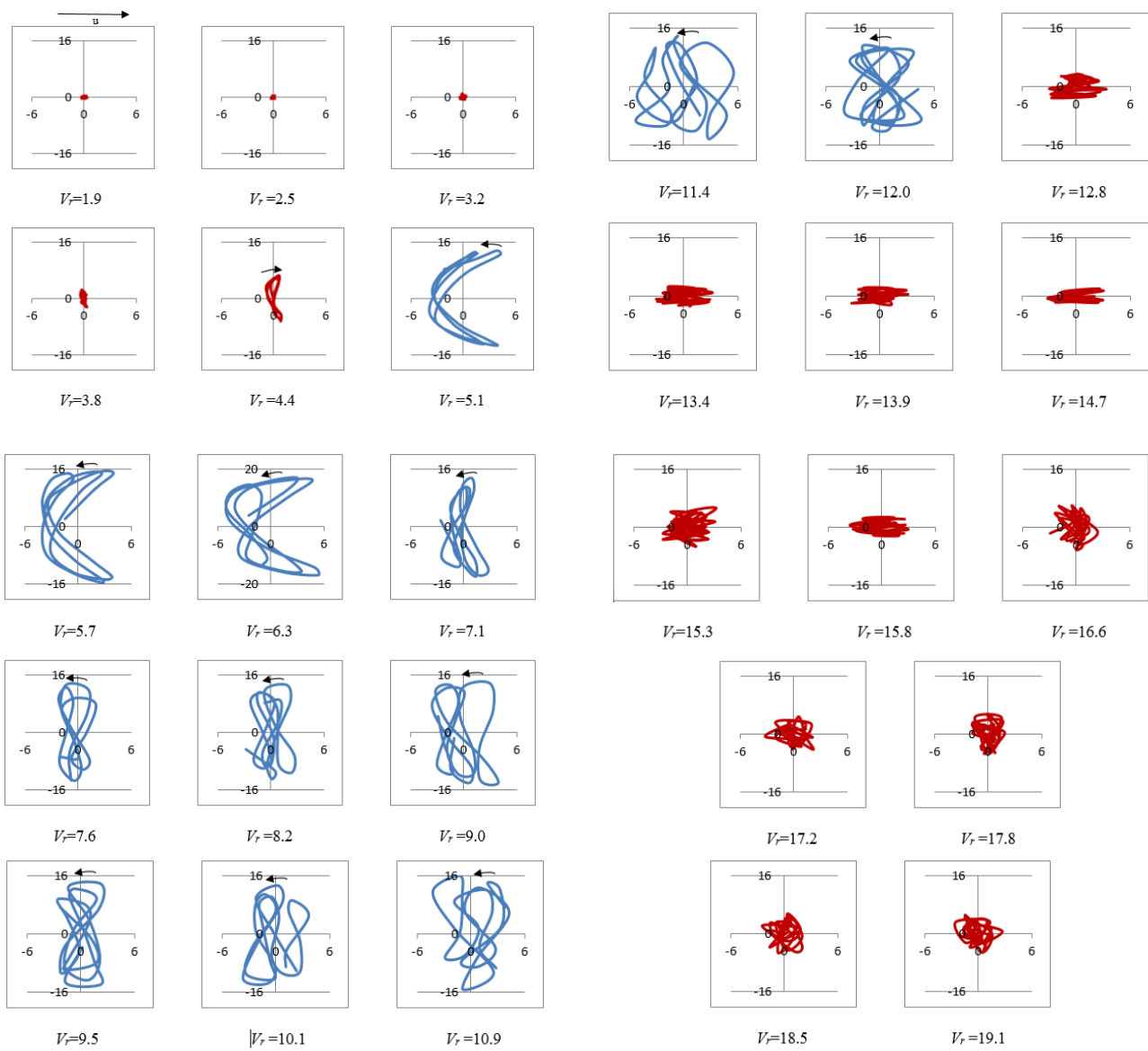


Fig. 5 Trajectory of flexible cylinder at various reduced velocity

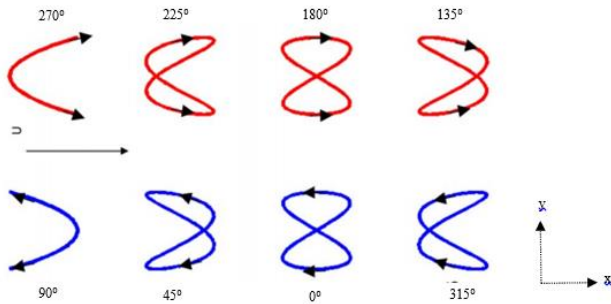


Fig. 6 IL and CF motion trajectories and its phase angle (reproduced from Vandiver *et al.* 2009)

3.4 Trajectory of the cylinder

The trajectory is obtained by taking the IL and CF displacement at the centre of the cylinder simultaneously. The trajectory of a flexible cylinder from 0.1 m/s to 1 m/s is shown in Fig. 5. It is plotted from 40 to 41 seconds for each of the velocities. The flow direction is from left to right. Based on Fig. 5, six different types of trajectories are found. Each of the changes of trajectory indicates the switch of the condition. From $V_r = 1.9$ to 2.5, the motion of the cylinder is very small. Hence, only a small dot is displayed in the trajectory where it denotes the non lock-in condition at low velocity. Starting from $V_r = 3.2$, the trajectory expands gradually until $V_r = 4.4$, where a crescent shape trajectory is formed. The crescent shape is amplified significantly from $V_r = 5.1$ to 6.3 before shifting the trajectory into 8-shape at $V_r = 7.0$. The expansion of the trajectory shows the initial branch while the occurrence of large crescent-shape represents the upper branch of the vibration. The 8-shape, which is designated in the lower branch, is continued until $V_r = 12.8$, where the IL displacement is started to be slightly larger than CF displacement (flat). The flat trajectory shows the buildup of a new higher mode of vibration. The condition changes again at $V_r = 16.6$, where slightly larger CF displacement is displayed. At this stage, the cylinder is dominated by second mode, where both sides of the cylinder vibrate vibrantly while only minor quiver is observed at the center of the cylinder (based on the observation of the cylinder during the experiment).

By observing Fig. 5, it can be seen that the trajectory is able to describe the motion of a cylinder clearly in IL and CF direction, especially during the lock-in region where the crescent and 8-shape trajectory can be easily noticed. Each change of the trajectory behaviour denotes the transition of the VIV phenomenon. However, limitation is found where the trajectory along the cylinder may be different from the center of the cylinder due to the lock-in of different dominant mode. Therefore, it can be only used as reference in predicting the occurrence of lock-in by referring to the types of the trajectories.

According to Vandiver *et al.* (2009), the shape of the trajectory depends on the phase angle, as shown in Fig. 6.

The CF is shown in y direction while the IL is indicated in x direction. Assuming the flow is in positive x direction, it can be seen that for the peak of the CF motion that are opposing to the flow, the trajectories are shown in blue.

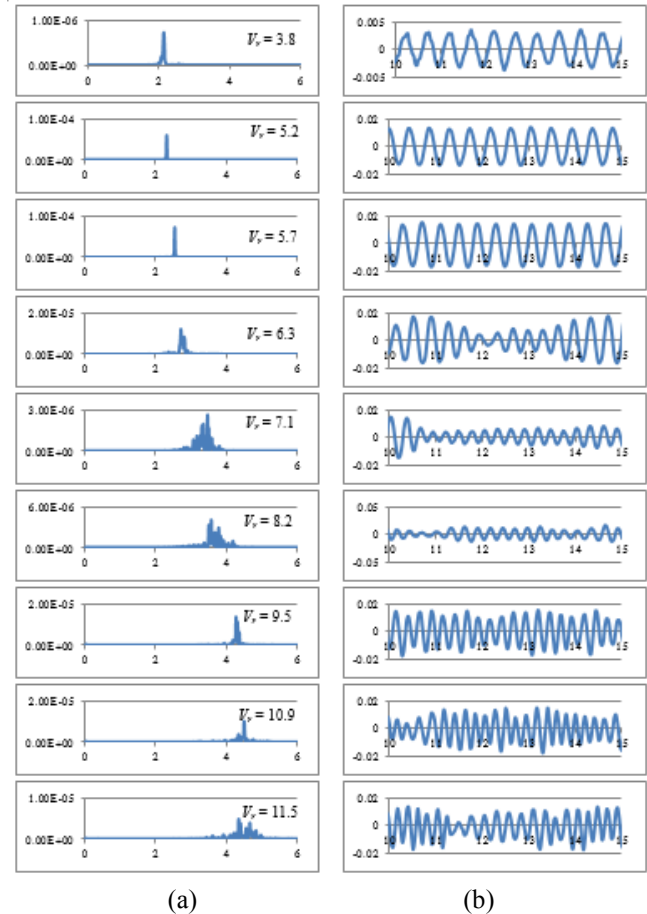


Fig. 7 Spectral response obtained from the hydrodynamic force of flexible cylinder with their corresponding time series of CF displacement at various velocity in the lock-in region ($3.8 < V_r < 11.5$). (a) the spectral response of hydrodynamic force; (b) the CF displacement in time series

These trajectories, from phase angle 315° to 90° , are very favourable to induce large VIV amplitude and lift forces (Dahl *et al.* 2007). This statement can be applied in Fig. 5 where starting from $V_r = 5.1$ which is under lock-in region, the cylinder motion is inverse with the flow direction and hence the trajectories are coloured in blue. The condition continues until $V_r = 12$ (lock-out region) where the CF motion starts to follow the direction of flow. This denotes that the vibration of the cylinder is not adequately strong to oppose the flow. Under this circumstance, they are unfavourable to substantial VIV (Vandiver *et al.* 2009), as shown in red in Fig. 5 and 6. With this information, the trajectories can be practiced as a useful tool in predicting the behaviour of VIV of a cylinder.

3.4.1 Power spectral density (PSD) of cylinder in lock-in region

The power spectral density (PSD) is described as the distribution of the signal power over the frequency of a cylinder. The PSD in CF direction can be obtained by transforming the CF strain data in time domain into frequency domain using Fast Fourier Transform (FFT), as explained in 3.4.2. Based on Fig. 7, the intensity of the PSD

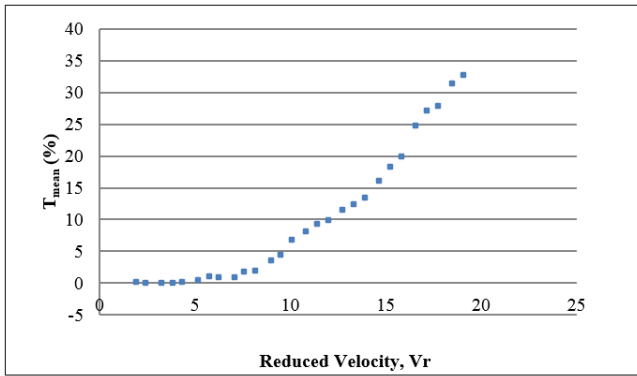


Fig. 8 Mean tension increase ratio (T_{mean}) of flexible cylinder at various reduced velocity

of hydrodynamic force (in y direction) is proportional to the amplitude. The larger the amplitude is, the larger the PSD intensity is. In addition, the PSD is found to be narrow-banded at the low velocity, while switching to broad-banded starting from $V_r = 6.3$ (Fig. 7). $V_r = 6.3$ is the transition point between the upper and lower branch. Therefore, it is believed that the vibration which is densely concentrated at single frequency at the upper branch is no longer retained at the lower branch, where the frequency is dispersed around the dominant frequency. This shows that the synchronization effect is the most severe at the upper branch compared with the lower branch.

3.5 Tension variation

In the offshore industry, the fluctuation of the tension is monitored constantly as it is one of the indications to detect the excessive fatigue or failure on cylinder. In the present study, pre-tension of 147N is applied to model a tension-dominated structure. A structure can be considered as tension-dominated if the IL vibration mode is twice of the CF mode whereas the IL-to-CF ratio is lower for an untensioned structure (Baarholm *et al.* 2006). During the runs of the experiment, tension varies due to the change of the velocity. The variation of the tension is investigated by observing the mean tension-increase ratio, which is obtained by dividing the increased tension by the pre-tension of a cylinder.

Based on Fig. 8, the relationship between the mean tension increase ratio and the reduced velocity of the cylinder follows a parabolic trend where the increment of tension is proportional to the square of the V_r . It can be understood that for a tension-dominated structure, the tension reacts as the reaction force to balance the increase of the induced drag forces with the reduced velocity along the cylinder. In the present study, the increment of 32% in tension variation is found to neutralize 21% of the drag increment. According to Chaplin *et al.* (2005), tension variation is highly related to the drag and the speed, where the increase of the carriage velocity increases the drag, and thus the tension.

Besides, based on equation 4, the increase of the mean tension increases the natural frequency (f_n) of the cylinder. Nevertheless, the percentage of change of the f_n is small,

where only 13% of the increment is found by increasing 32% of the mean tension. The increase of the mean tension is about 2.5-fold of the f_n .

$$\sqrt{\left(\frac{n}{2}\right)^2 \frac{T}{mL^2} + \left(\frac{n^2\pi}{2}\right)^2 \frac{EI}{mL^2}} \approx f_n \quad n=1,2,3, \dots \quad (4)$$

3.6 Hydrodynamic coefficients

Hydrodynamic forces are commonly evaluated in terms of fluctuating drag force coefficient ($C_{d,fluc}$), fluctuating lift force coefficient ($C_{l,fluc}$) and mean drag force coefficient ($C_{d,mean}$). The $C_{d,mean}$ and the fluctuating terms of $C_{d,fluc}$ and $C_{l,fluc}$ can be attained by dividing the force data in term of mean and standard deviation with the length of the cylinder that were exposed to velocity. They are expressed in equation 5,6 and 7 respectively.

$$C_{d,mean} = \frac{F_{d,mean}}{1/2\rho u^2 LD} \quad (5)$$

$$C_{d,fluc} = \frac{F_{d,std}}{1/2\rho u^2 LD} \quad (6)$$

$$C_{l,fluc} = \frac{F_{l,std}}{1/2\rho u^2 LD} \quad (7)$$

$F_{d,mean}$, denotes the mean drag force, $F_{d,std}$ and $F_{l,std}$ represent standard deviation of drag force and standard deviation lift force, respectively. These forces are decomposed from the total forces. D , L , ρ and u represent the diameter of cylinder, the length of cylinder, the density and the flow velocity, respectively. In the analysis, because of the enormous initial forces results in huge drag coefficient, the drag data at 0.1 m/s is discarded.

3.6.1 Mean drag coefficient

Fig. 9 indicates the $C_{d,mean}$ of a flexible cylinder at various reduced velocity. At the initial and upper branches, the $C_{d,mean}$ is found in between values of 1.9 and 3.1. The highest value is found at the upper branch, right after the occurrence of maximum amplitude. After the maximum value, the $C_{d,mean}$ drops rapidly in the lower branch, before increasing slightly and maintain the values in between 2.5 and 2.9. It is believed that the amplification of the $C_{d,mean}$ is due to the large amplitude response under lock-in condition. In fact, similar conditions are also reported by Huera-Huarte and Bearman (2009b).

Good agreement is found for the $C_{d,mean}$ of the flexible cylinder in the present study (Fig. 10) with the experimental data of Huera-Huarte and Bearman (2009) and Sanaati and Kato (2012). Throughout the entire velocity range, the average $C_{d,mean}$ in the present study is found to be 2.654. This value is higher than the short rigid cylinder that experiencing force and free motions. Similar condition was also reported by Huera-Huarte *et al.* (2014) (Fig. 10) where the $C_{d,mean}$ of a flexible cylinder was larger than three under the stepped flow. The similarity between these studies is that pre-tension is applied with the use of flexible cylinder. Based on Fig. 10, it is found that the increase of the pre-tension increases the $C_{d,mean}$. This suggests that the pre-tension applied on the flexible cylinder has direct

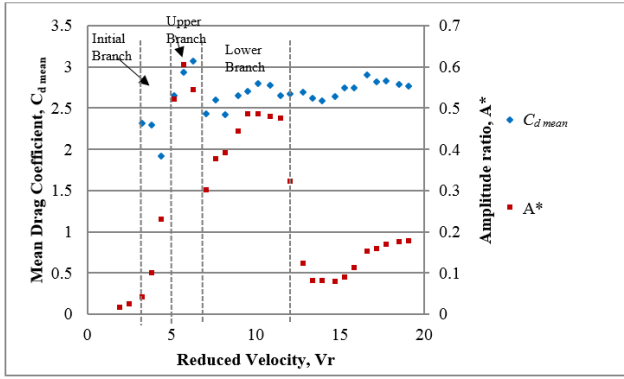


Fig. 9 Mean drag coefficient and amplitude response of flexible cylinder at various reduced velocity

relationship with the drag. In fact, by referring to the beam equation subjected to static axial loading (pre-tension) $T(x)$ (Equation 8), the increase of pre-tension increases the dynamic lateral loading $p(x,t)$ if the other parameters are assumed to be constant.

$$m(x) \frac{\partial^2 w(x,t)}{\partial t^2} - \frac{\partial}{\partial x} \left(T(x) \frac{\partial w(x,t)}{\partial x} \right) + \frac{\partial^2}{\partial x^2} \left(EI(x) \frac{\partial^2 w(x,t)}{\partial x^2} \right) = p(x,t) \quad (8)$$

The $m(x)$ and $EI(x)$ in Equation 8 denote the mass per unit length and the bending stiffness, respectively for a beam, while $w(x,t)$ is the displacement response.

In explaining the reason that the $C_{d,mean}$ of a flexible cylinder is larger than the rigid circular cylinder, the following equation can be referred to (Huera-Huarte and Bearman (2009)).

$$\frac{C_D}{C_{D0}} = 1 + 1.6 \left(\frac{\sigma_y}{D} \right)^{0.4} \quad (9)$$

In the equation, the $C_{d,mean}$ of a flexible cylinder is normalized with the mean drag coefficient of a stationary cylinder, while σ_y is the standard deviation of the CF motion. This equation can be used to predict the drag coefficient for cases of lock-in of a flexible cylinder (Vandiver, 1983). The equation shows that the CF amplitude response has a direct relationship with the $C_{d,mean}$, where the larger CF amplitude response in a flexible cylinder will result in the larger value of $C_{d,mean}$. This can also be used to rationalize the large $C_{d,mean}$ of flexible cylinder compared to a rigid cylinder.

3.6.2 Fluctuating lift and drag coefficients

The oscillating force is originally induced by the vortex shedding. The vortices are generated as the current flows around a cylinder. This condition causes the changes on the pressure distribution around the cylinder periodically. This pressure change result in the periodic force variation. These forces is usually defined as fluctuating force coefficients. In the present study, the fluctuating lift and drag forces are investigated to identify the intensity of the oscillation in CF and IL directions, respectively.

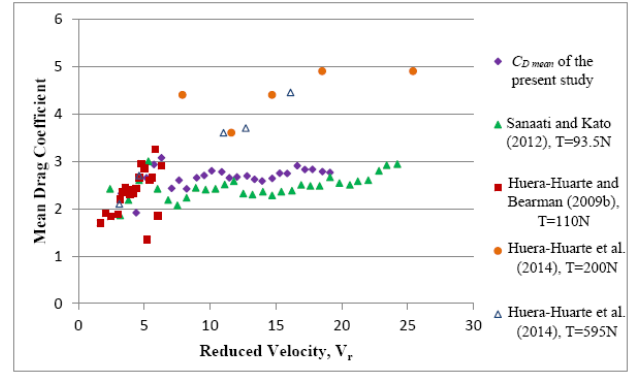


Fig. 10 Mean drag coefficient against the reduced velocity of various previous studies.

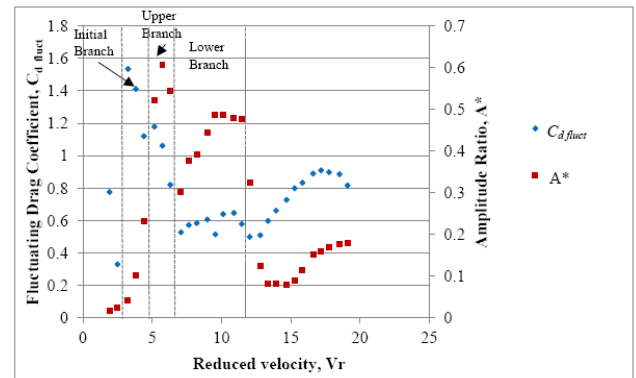


Fig. 11 Fluctuating drag coefficient of flexible cylinder at various reduced velocity

Based on Fig. 11, the maximum $C_{d,fluct}$ of flexible cylinder with value around 73% of the average $C_{d,mean}$, is found to occur at the entering point of CF lock-in region, $V_r = 3.2$. Another $C_{d,fluct}$ peak with relatively smaller value is found at $V_r = 5.2$. As the V_r increases, the $C_{d,fluct}$ is reduces gradually until a constant value is reached. Starting from $V_r = 12$, the $C_{d,fluct}$ increases slightly once more as the secondary CF lock-in occurs, showing that the $C_{d,fluct}$ is greatly affected by the synchronization.

The large increase of the $C_{d,fluct}$ at the initial branch rather than upper branch indicates that the occurrence of the maximum oscillation in the IL and CF directions are not simultaneous. In fact, the maximum IL oscillation takes place earlier than the CF oscillation. Similar condition was also reported by Sarpkaya (2004).

In general, $C_{l,fluct}$ is used to describe the vortex shedding process. At low V_r , the vortex shedding is weak, resulting in the low values of $C_{l,fluct}$. For a stationary cylinder that allows moving in CF only, the $C_{l,fluct}$ starts to increase at $Re \approx 1600$ (Norberg, 2003). Similar conditions are observed in the present study, but these processes are shifted slightly to larger Reynolds number for a flexible cylinder.

For a low mass ratio flexible cylinder, the increment of $C_{l,fluct}$ starts at $V_r = 3.2$ ($Re \approx 3000$) while rapid increment is found at $V_r = 4.4$ (Fig. 12). The increase of $C_{l,fluct}$ is because the transition-to-turbulence separation point is in parallel with the wake closure in streamwise position (Roshko, 1993). The process of transition to turbulence has its

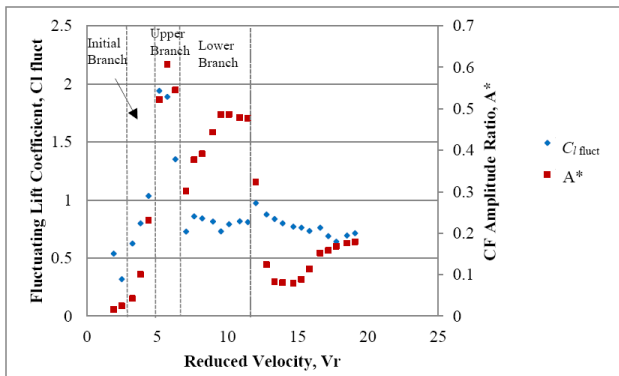


Fig. 12 Fluctuating lift coefficient of flexible cylinder at various reduced velocity

own wake development, called rib-like secondary vortices, which is known as mode B vortices. As the mode B vortices are in concurrence with the shear-layer vortices, the maximum $C_{l\ fluct}$ is achieved (Norberg, 2001). The high values of $C_{l\ fluct}$ also indicate the strong vortex shedding with substantial spanwise correlation (Norberg, 2003). The $C_{l\ fluct}$ is then reduced significantly to a constant value (around 0.8) after reaching the maxima. It is because the mode B vortices are no longer in harmony with the shear layer vortices, causing the decrement of the correlation in spanwise.

4. Conclusion

Laboratory experiment of a low mass ratio and high aspect ratio flexible cylinder is performed in the towing tank at Osaka University. For a flexible cylinder with low mass ratio, four branches namely initial, upper, lower and desynchronization are observed. The synchronization region is found, which is broad-banded with larger amplitude compared to a rigid cylinder with high mass ratio. The main reason is due to the added mass effect where the difference in added mass results in an increment of the apparent natural frequency for a low mass ratio cylinder. In addition, the flexibility of the cylinder end condition allows the cylinder to vibrate with larger amplitude.

A smaller Strouhal number, $St=0.158$ is obtained in the present study. Large IL-to-CF frequency ratio shows the strong influence of IL mode on the CF frequency response. Each of the frequency switches represents the change of VIV phenomenon such as the change of the branches, formation of higher mode and the transition between different VIV behaviour.

The mean tension increase rate is in parabolic trend with the increase of the Vr . It is because the tension is correlated with the velocity and drag. The highest $Cd\ mean$ is found in the upper branch, which is due to the large amplitude response under lock-in. The maximum oscillation of IL and CF directions occurs at dissimilar periods. In the present study, the maximum CF oscillation takes place later than the IL oscillation. Besides, the increment of the CF oscillation of a flexible cylinder is shifted to larger Re .

Acknowledgments

This research was financially supported by Japan International Cooperation Agency under grant (S.K130000.0543.4Y191) and Universiti Teknologi Malaysia research grant (R.K130000.7343.4B362).

References

- Aguirre, J.E. (1978), "Flow Induced, In-line Vibrations of a Circular Cylinder". Ph.D. Dissertation, Imperial College of Science and Technology, London, United Kingdom.
- Assi, G.R.S. (2009), "Mechanisms for flow-induced vibration of interfering bluff bodies". Ph.D. Dissertation, Imperial College, London, United Kingdom.
- Baarholm, G.S., Larsen, C.M. and Lie, H. (2006), "On fatigue damage accumulation from in-line and cross-flow vortex-induced vibrations on risers", *J. Fluids Struct.*, **22**, 109-127. <https://doi.org/10.1016/j.jfluidstructs.2005.07.013>
- Bearman, P.W. (2011), "Circular cylinder wakes and vortex-induced vibrations", *J. Fluids Struct.*, **27**, 648-658. <https://doi.org/10.1016/j.jfluidstructs.2011.03.021>
- Blevins, R.D. and Coughran, C.S. (2009), "Experimental Investigation of vortex-induced vibration in one and two dimensions with variable mass, damping, and Reynolds number", *J. Fluids Eng.*, **131**, 10, 101202. <https://doi.org/10.1115/1.3222904>.
- Boom, H.J.J. and Walree, F. (1990), "Hydrodynamic aspects of flexible risers", *Offshore Technology Conference (OTC)*, Houston, Texas, May.
- Branković, M., and Bearman, P. (2006), "Measurements of transverse forces on circular cylinders undergoing vortex-induced vibration", *J. Fluids Struct.*, **22**(6), 829-836. <https://doi.org/10.1016/j.jfluidstructs.2006.04.022>.
- Chaplin, J.R., Bearman, P.W., Huará Huarte, F.J. and Pattenden, R.J. (2005), "Laboratory measurements of vortex-induced vibrations of a vertical tension riser in a stepped current", *J. Fluids Struct.*, **21**, 3-24. <https://doi.org/10.1016/j.jfluidstructs.2005.04.010>
- Chen, W., Ji, C., Mahbub Alam, M. and Xu, D. (2019), "Flow-induced vibrations of three circular cylinders in an equilateral triangular arrangement subjected to cross-flow", *Wind Struct.*, **29**, 43-53. <https://doi.org/10.12989/was.2019.29.1.043>.
- Currie, I.G. and Turnbull, D.H. (1987), "Streamwise oscillations of cylinders near the critical Reynolds number". *J. Fluids Struct.*, **1**, 185-196. [https://doi.org/10.1016/S0889-9746\(87\)90331-8](https://doi.org/10.1016/S0889-9746(87)90331-8).
- Dahl, J.M., Hover, F.S. and Triantafyllou, M.S. (2006), "Two-degree-of-freedom vortex-induced vibrations using a force assisted apparatus", *J. Fluids Struct.*, **22**, 807-818. <https://doi.org/10.1016/j.jfluidstructs.2006.04.019>.
- Dahl, J.M., Hover, F.S., Triantafyllou, M.S., Dong, S. and Karniadakis, G.E. (2007), "Resonant vibrations of bluff bodies cause multi-vortex shedding", *Physic Rev. Lett.*, **99**, 144503. <https://doi.org/10.1103/PhysRevLett.99.144503>.
- Dahl, J.J.M. (2008), "Vortex-induced vibration of a circular cylinder with combined in-line and cross-flow motion", Ph.D. Dissertation, Massachusetts Institute of Technology, USA.
- Dahl, J.M., Hover, F.S., Triantafyllou, M.S. and Oakley, O.H. (2010), "Dual resonance in vortex-induced vibrations at subcritical and supercritical Reynolds number", *J. Fluid Mech.*, **643**, 395-424. <https://doi.org/10.1017/S0022112009992060>.
- Feng, C.C. (1968), "The measurement of vortex induced effects in flow past stationary and oscillating circular and D-section cylinders", M.Sc. Dissertation, Department of Mechanical Engineering, The University of British Columbia, Canada.

- Gabbai, R.D. and Benaroya, H. (2005), "An overview of modeling and experiments of vortex-induced vibration of circular cylinders", *J. Sound Vib.*, **282**, 575-616. <https://doi.org/10.1016/j.jsv.2004.04.017>.
- Gonçalves, R.T., Rosetti, G.F., Franzini, G.R., Meneghini, J.R., Fajarra, A.L.C. (2013), "Two-degree-of-freedom vortex-induced vibration of circular cylinders with very low aspect ratio and small mass ratio", *J. Fluids Struct.*, **39**, 237-257. <https://doi.org/10.1016/j.jfluidstructs.2013.02.004>
- Govardhan, R. and Williamson, C.H.K. (2000), "Modes of vortex formation and frequency response of a freely vibrating cylinder", *J. Fluid Mech.*, **420**, 85-130. <https://doi.org/10.1017/S0022112000001233>.
- Han, Q., Ma, Y., Xu, W., Lu, Y. and Cheng, A. (2017), "Dynamic characteristics of an inclined flexible cylinder undergoing vortex-induced vibrations", *J. Sound Vib.*, **394**, 306-320. <https://doi.org/10.1016/j.jsv.2017.01.034>.
- Huera Huarte, F.J. (2006), "Multi-mode vortex-induced vibrations of a flexible circular cylinder", Ph.D. Dissertation, Department of Aeronautics, Imperial College London, United Kingdom.
- Huera-Huarte, F.J. and Bearman, P.W. (2009), "Wake structures and vortex-induced vibrations of a long flexible cylinder-Part 2: Drag coefficients and vortex modes", *J. Fluids Struct.*, **25**, 991-1006. <https://doi.org/10.1016/j.jfluidstructs.2009.03.006>
- Huera-Huarte, F.J., Bangash, Z.A., Gonzalez, L.M. (2014), "Towing tank experiments on the vortex-induced vibrations of low mass ratio long flexible cylinders", *J. Fluids Struct.*, **48**, 81-92. <https://doi.org/10.1016/j.jfluidstructs.2014.02.006>.
- Huse, E., Nielsen, F.G. and Soreide, T. (2002), "Coupling between in-line and transverse VIV response", *ASME 21st International Conference on Offshore Mechanics and Arctic Engineering OMAE2002-28618*, Oslo, Norway, June.
- Jauvtis, N. and Williamson, C.H.K. (2003), "Vortex-induced vibration of a cylinder with two degrees of freedom", *J. Fluids Struct.*, **17**, 1035-1042. [https://doi.org/10.1016/S0889-9746\(03\)00051-3](https://doi.org/10.1016/S0889-9746(03)00051-3).
- Jauvtis, N. and Williamson, C.H.K. (2004), "The effect of two degrees of freedom on vortex-induced vibration at low mass and damping", *J. Fluid Mech.*, **509**, 23-62. <https://doi.org/10.1017/S0022112004008778>
- Jeong, Y., Park, M. and You, Y. (2016), "Experimental study on wave forces to offshore support structures", *Struct. Eng. Mech.*, Vol. **60**, 193-209. <https://doi.org/10.12989/sem.2016.60.2.193>
- Jus, Y., Longatte, E., Chassaing, J.C. and Sagaut, P. (2014), "Low Mass-Damping Vortex-Induced Vibrations of a Single Cylinder at Moderate Reynolds Number", *J. Press Vessel Technol.*, **136**(5), 0513051-513057. <https://doi.org/10.1115/1.4027659>.
- Ji, C., Peng, Z., Mahbub Alam, M., Chen, W. and Xu, D. (2018), "vortex-induced vibration of a long flexible cylinder in uniform cross-flow", *Wind Struct.*, **26**, 267-277. <https://doi.org/10.12989/was.2018.26.5.267>
- Kang, H.S., Kim, M.H., Aramanadka, S.S.B., Kang, H.Y. and Lee, K.Q. (2017), "Suppression of tension variations in hydro-pneumatic riser tensioner by using force compensation control", *Ocean Syst. Eng.*, **7**, 225-246. <https://doi.org/10.12989/ose.2017.7.3.225>
- Khalak, A. and Williamson, C.H.K. (1997), "Fluid forces and dynamics of a hydroelastic structure with very low mass and damping", *J. Fluids Struct.*, **11**, 973-982. <https://doi.org/10.1006/jfls.1997.0110>
- Khalak, A. and Williamson, C.H.K. (1999), "Motions, forces and mode transitions in vortex-induced vibrations at low mass-damping", *J. Fluids Struct.*, **13**, 813-851. <https://doi.org/10.1006/jfls.1999.0236>
- Kim, D.K., Choi, H.S., Shin, C.S., Liew, M.S., Yu, S.Y. and Park, K.S. (2015), "Fatigue performance of deepwater SCR under short-term VIV considering various S-N curves", *Struct. Eng. Mech.*, **53**, 881-896. <https://doi.org/10.12989/sem.2015.53.5.881>.
- Korkischko, I. and Meneghini, J.R. (2010), "Experimental investigation of flow-induced vibration on isolated and tandem circular cylinders fitted with strakes", *J. Fluids Struct.*, **26**, 611-625. <https://doi.org/10.1016/j.jfluidstructs.2010.03.001>
- Kuiper, G.L. (2008), "Stability of offshore risers conveying fluid", Ph.D. Dissertation, Delft, Eburon Uitgeverij.
- Lee, K.Q., Abu, A. and Muhamad, P. (2013), "Investigation of wide range of flow around circular cylinder using turbulence model", *Adv. Mater. Res.*, **664**, 878-883. <https://doi.org/10.4028/www.scientific.net/AMR.664.878>.
- Marcollo, H. and Hinwood, J.B. (2006), "On shear flow single mode lock-in with both cross-flow and in-line lock-in mechanisms", *J. Fluids Struct.*, **22**, 197-211. <https://doi.org/10.1016/j.jfluidstructs.2005.10.001>.
- Naomi Kato (1982), "A study on separated flows behind bluff bodies by inviscid vortex models (2nd report)", *J. Soc. Naval Architects Japan*, **151**, 15-22. <https://doi.org/10.2534/jjasnaoe1968.1982.15>.
- Norberg, C. (2001), "Flow around a circular cylinder: Aspects of fluctuating lift", *J. Fluids Struct.*, **15**, 459-469. <https://doi.org/10.1006/jfls.2000.0367>.
- Norberg, C. (2003), "Fluctuating lift on a circular cylinder: review and new measurements", *J. Fluids Struct.*, **17**, 57-96. [https://doi.org/10.1016/S0889-9746\(02\)00099-3](https://doi.org/10.1016/S0889-9746(02)00099-3).
- Quen, L.K., Abu, A., Kato, N., Muhamad, P., Sahekhaini, A., Abdullah, H. (2014), "Investigation on the effectiveness of helical strakes in suppressing VIV of flexible riser", *Appl. Ocean Res.*, **44**, 82-91. <https://doi.org/10.1016/j.apor.2013.11.006>.
- Rahman, M.A., Leggoe, J., Thiagarajan, K., Mohd, M.H. and Paik, J.K. (2016), "Numerical simulations of vortex-induced vibrations on vertical cylindrical structure with different aspect ratios", *Ships Offshore Struct.*, **11**(4), 405-423. <https://doi.org/10.1080/17445302.2015.1013783>.
- Roshko, A. (1961), "Experiments on the flow past a circular cylinder at very high Reynolds number", *J. Fluid Mech.*, **10**(3), 345-356. <http://dx.doi.org/10.1017/S0022112061000950>.
- Roshko, A. (1993), "Perspectives on bluff body aerodynamics", *J. Wind Eng. Industrial Aerodynam.*, **49**, 79-100. [https://doi.org/10.1016/0167-6105\(93\)90007-B](https://doi.org/10.1016/0167-6105(93)90007-B).
- Sanaati, B. (2012), "An experimental study on the VIV hydrodynamics of pre-tensioned flexible cylinders with single and multiple configurations", Ph.D. Dissertation, Osaka University, Japan.
- Sanaati, B. and Kato, N. (2012), "A study on the effects of axial stiffness and pre-tension on VIV dynamics of a flexible cylinder in uniform cross-flow", *Appl. Ocean Res.*, **37**, 198-210. <https://doi.org/10.1016/j.apor.2012.05.001>.
- Sanchis, A., Sælevik, G. and Grue, J. (2008), "Two-degree-of-freedom vortex-induced vibrations of a spring-mounted rigid cylinder with low mass ratio", *J. Fluids Struct.*, **24**, 907-919. <https://doi.org/10.1016/j.jfluidstructs.2007.12.008>.
- Sarpkaya, T. (2004), "A critical review of the intrinsic nature of vortex-induced vibrations", *J. Fluids Struct.*, **19**, 389-447. <https://doi.org/10.1016/j.jfluidstructs.2004.02.005>.
- Song, L., Fu, S., Dai, S., Zhang, M. and Chen, Y. (2016), "Distribution of drag force coefficient along A flexible riser undergoing VIV in sheared flow", *Ocean Eng.*, **126**, 1-11. <https://doi.org/10.1016/j.oceaneng.2016.08.022>.
- Vandiver, J.K. (1983), "Drag coefficients of long flexible cylinders", *Offshore Technology Conference*, Texas, USA, May.
- Vandiver, J.K. (1993), "Dimensionless parameters important to the prediction of vortex-induced vibration of long, flexible cylinders in ocean currents", *J. Fluids Struct.*, **7**, 292-308. <https://doi.org/10.1006/jfls.1993.1028>.
- Vandiver, J. K. (1998), "Research challenges in the vortex-induced vibration prediction of marine risers", *Offshore Technology*

Conference (OTC), Houston, USA, May.

- Vandiver, J.K., Jaiswal, V. and Jhingran, V. (2009), "Insights on vortex-induced, travelling waves on long risers", *J. Fluids Struct.* **25**, 641-653. <https://doi.org/10.1016/j.jfluidstructs.2008.11.005>.
- Vikestad, K., Vandiver, J.K. and Larsen, C.M. (2000), "Added mass and oscillation frequency for a circular cylinder subjected to vortex-induced vibrations and external disturbance", *J. Fluids Struct.*, **14**, 1071-1088. <https://doi.org/10.1006/jfls.2000.0308>.
- Williamson, C.H.K. and Roshko, A. (1988), "Vortex formation in the wake of an oscillating cylinder", *J. Fluids Struct.*, **2**, 355-381. [https://doi.org/10.1016/S0889-9746\(88\)90058-8](https://doi.org/10.1016/S0889-9746(88)90058-8).
- Williamson, C.H.K. and Govardhan, R. (2008), "A brief review of recent results in vortex-induced vibrations", *J. Wind Eng. Industrial Aerodynam.*, **96**, 713-735. <https://doi.org/10.1016/j.jweia.2007.06.019>
- Wu, J., Lie, H., Larsen, C.M., Liapis, S. and Baarholm, R. (2016), "Vortex-induced vibration of a flexible cylinder: Interaction of the in-line and cross-flow responses", *J. Fluids Struct.* **63**, pp. 238 – 258. <https://doi.org/10.1016/j.jfluidstructs.2016.03.001>
- Xu, J., He, M., Bose, N. (2009), "Vortex modes and vortex-induced vibration of a long, flexible riser", *Ocean Eng.* **36**, 456-467. <https://doi.org/10.1016/j.oceaneng.2009.01.010>
- Xu, W., Qin, W., Gao, X. (2018), "Experimental Study on Streamwise Vortex-Induced Vibration of a Flexible Slender Cylinder", *Appl. Sci.* **8**, 311. doi:10.3390/app8020311

CC